# Dielectric-Insensitive Phased Array with Improved Characteristics for 5G Mobile Handsets

*Progress In Electromagnetics Research M, Vol. 94, 209–219, 2020*

# Dielectric-Insensitive Phased Array with Improved Characteristics for 5G Mobile Handsets

**Naser O. Parchin[1, *], Haleh J. Basherlou[2], and Raed A. Abd-Alhameed[1]**

**Abstract**—In this manuscript, a dielectric-insensitive beam-steerable phased array antenna with improved performance is introduced for fifth-generation (5G) mobile handsets. The configuration of the design is arranged by employing eight dielectric-insensitive L-ring/slot-loop radiators in a linear form on the top edge of the handset mainboard. The beam-steerable array design exhibits high radiation performances even though it is implemented on a lossy FR-4 material. The proposed design exhibits an impedance bandwidth of 18–20 GHz with the center frequency of 19 GHz. It provides satisfactory characteristics such as wide beam-steering, high gain, and efficiency characteristics indicating its promising potential for beam-steerable 5G smartphones. The characteristics of the antenna array are insensitive for different types of dielectrics. Furthermore, the designed antenna array offers quite good radiation behavior in the presence of hand phantom.

## 1. INTRODUCTION

The fifth-generation (5G) wireless network has received a lot of attention from both academia and industry with many reported efforts [1–5]. It is expected to have significant improvements in terms of transmission rate, mobility,latency, and so on [6–8]. Compacted with 3G/4G communications, one of the main challenges in 5G networks is to shift to the higher frequencies(beyond 10 GHz) where it is easier to obtain wider impedance bandwidths and higher data rates [9–12]. 5G is predicted to provide an aggregate data rate, 1,000 times faster than 4G networks with better reliability. Different trials of 5G demo systems are carried out with multiple mobile technology corporations involved [13]. 5G systems will employ phased array antennas in the user equipment (UE) and the base station (BS) [14–20]. So many challenges have been reported for using high frequencies in antenna components of 5G wireless devices. One of the challenges is to implement antenna phased arrays with improved radiation performances [21–25]. Phased array antennas with high performances are very desirable for 5G cellular networks since they can improve the connectivity and the efficiency of the 5G systems [26–29].

In this paper, a new phased array with high performance and dielectric-insensitive function for 5G smartphone applications is proposed. This is achieved by arranging eight dielectric-insensitive radiators in a linear form on the top edge of the handset mainboard. A dielectric-insensitive radiator can be obtained by employing a metal-ring radiator inside an air-filled dielectric. Since the main dielectric of the antenna elements is the air, they exhibit high characteristics in terms of antenna gain and efficiency. Moreover, the antenna is insensitive for various values of loss tangent characteristics and permittivity, which make it flexible to be designed in different dielectric types. Characteristics of the single-element resonator and suitable the phased array design are investigated in the following.

*Received 21 April 2020, Accepted 14 July 2020, Scheduled 2 August 2020*

* Corresponding author: Naser Ojaroudi Parchin (N.OjaroudiParchin@bradford.ac.uk).

[1] Faculty of Engineering and Informatics, University of Bradford, Bradford BD7 1DP, UK. [2] Bradford College, Bradford BD7 1AY, UK.

## 2. CHARACTERISTICS OF THE SINGLE-ELEMENT ANTENNA

Figures 1(a)and (b) plot the side and front views of the air-filled L-ring antenna. It is designed on a low-cost FR-4 dielectric with characteristics of $h_{sub} = 0.8\,\text{mm}$, loss tangent ($\delta$) = 0.025, and dielectric constant (permittivity = $\varepsilon_r$) of 4.3. It should be noted that FR4 is too lossy for millimeter-wave/centimeter-wave antenna designs with traditional structures such as printed patch antenna, where the efficiency of the antenna would be deteriorated. However, the proposed design technique could eliminate the effect of high-loss substrate and improve the antenna performance.As shown, a discrete-feeding port is used across the center of the L-ring radiator to feed the proposed antenna. The CST Microwave software is used to study the characteristics of the designed antenna [30]. The $S_{11}$ characteristic of the simulated L-ring slot-loop antenna is illustrated in Fig. 1(b). As can be observed, the designed antenna works at the frequency range from 18 to 20 GHz (with 2 GHz impedance bandwidth). The values of the antenna design parameters are specified in Table 1.

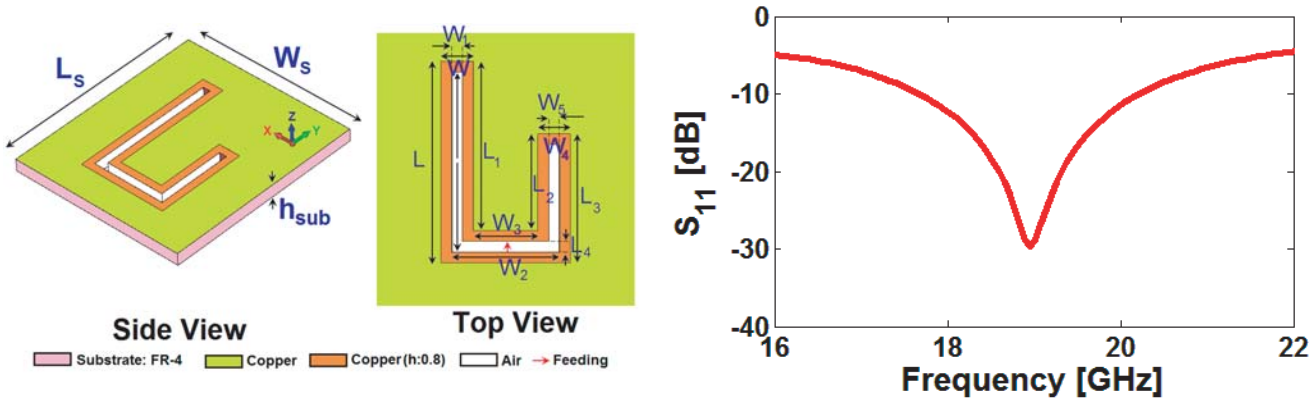


(a) (b)

**Figure 1.** (a) Configuration (b) $S_{11}$ result of the air-filled slot-loop element.

**Table 1.** The dimensions of the designed parameters for the 5G antenna and its array.

| Param. | $W_{sub}$ | $L_{sub}$ | $h_{sub}$ | $W_S$ | $L_S$ | $W$ | $L$ | $W_1$ | $L_1$ |
|---|---|---|---|---|---|---|---|---|---|
| (mm) | 55 | 110 | 0.8 | 12 | 13.5 | 1.5 | 9.5 | 0.5 | 8 |
| Param. | $W_2$ | $L_2$ | $W_3$ | $L_3$ | $W_4$ | $L_4$ | $W_5$ | $L_a$ | $W_a$ |
| (mm) | 5 | 4.5 | 3 | 6 | 1.5 | 0.5 | 0.5 | 10.5 | 51.5 |

The current density for the L-ring slot resonator at its resonance frequency (19 GHz) is plotted in Fig. 2(a). As seen, the employed metal-ring radiator has high current densities and emerges very active at the target frequency [31–35]. The 3D radiation pattern of the metal-ring design is shown in Fig. 2(b). It is seen that the presented dielectric-insensitive antenna has quite good radiation, supporting both the top and bottom sides of the FR-4 dielectric. In addition, it provides a high realized gain of 5 dB. Fig. 3(a) shows the maximum gain and efficiencies of the antenna over its operating frequency. As shown, radiation and total efficiencies of the design are almost equal with the value of $-0.25\,\text{dB}$ (95%) at 19 GHz. Besides, the maximum gain of the antenna is almost constant with 5 dBi level at 19 GHz. In order to demonstrate the advantage and high-efficiency function of the presented antenna design compared with other antennas, the characteristics of a 19 GHz patch antenna with the same dimension of the substrate, operation frequency, and properties of the dielectric is investigated and compared. Fig. 3(b) shows and compares the radiation and total efficiencies of the antennas (conventional 19 GHz patch antenna and the air-filled slot design) over their frequency bands. It is clearly shown that by employing the proposed design method, the efficiencies of an antenna radiator can be significantly improved. Besides, the design configuration and reflection coefficient ($S_{11}$) of the conventional 19 GHz patch antenna are shown in

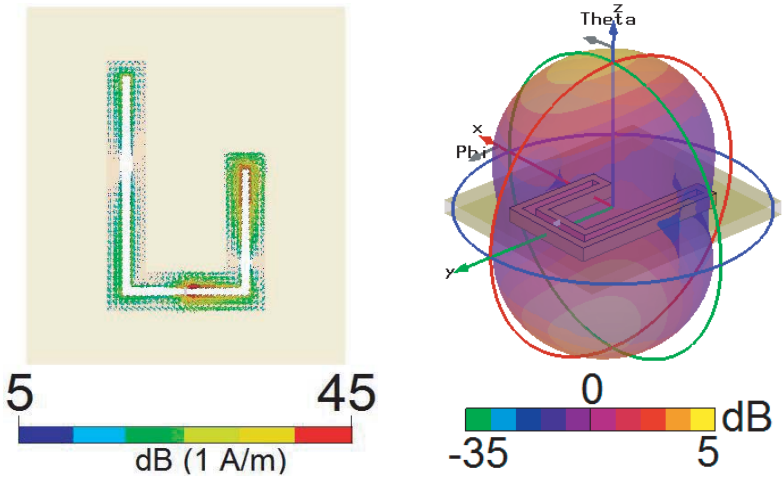


(a) (b)

**Figure 2.** (a) The current distribution and (b) 3D radiation at 19 GHz.

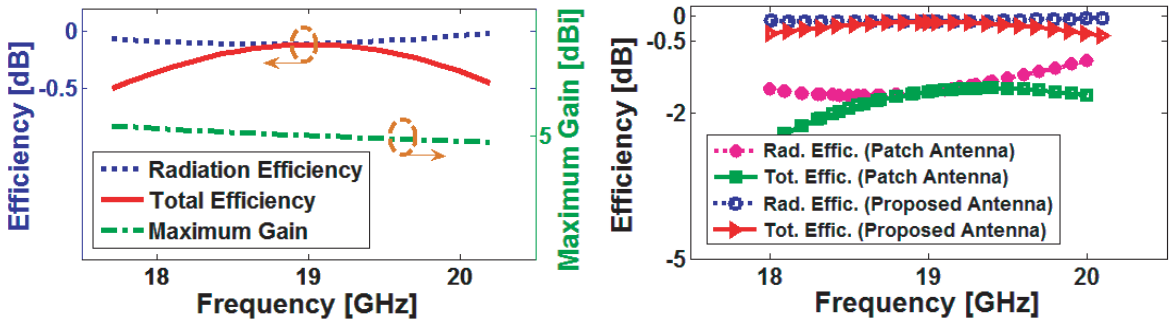


(a) (b)

**Figure 3.** (a) Radiation properties over the operation band and (b) comparison between efficiencies of the antenna and the conventional patch antenna.

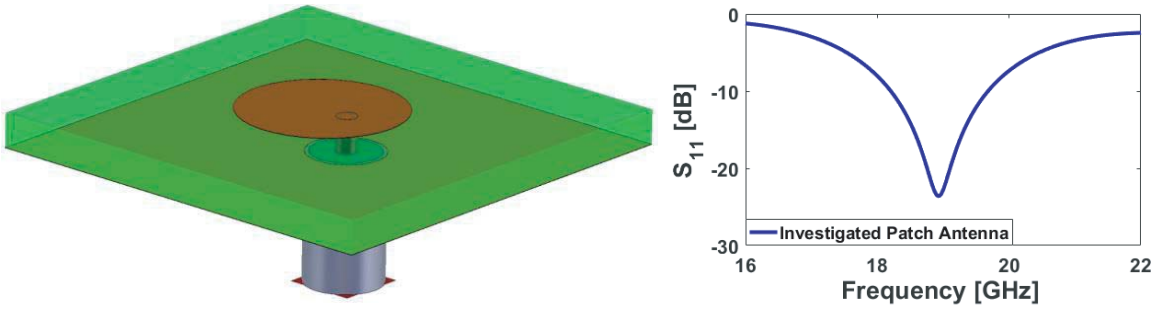


(a) (b)

**Figure 4.** (a) Configuration and (b) $S_{11}$ results of the investigated 19 GHz patch antenna.

Figs. 4(a) and (b), respectively. The circular radiation patch has a compact size with a diameter of 3.9 mm and it is fed by a coaxial cable [36, 37]. As mentioned above, the properties of the proposed air-filled slot antenna design are insensitive to different dielectric characteristics.

To further understand this function, the reflection coefficient ($S_{11}$) and total efficiencies of the antenna element for different dielectrics including FR-4 ($\delta = 0.025$ & $\varepsilon_r = 4.3$), Arlon Ad-320

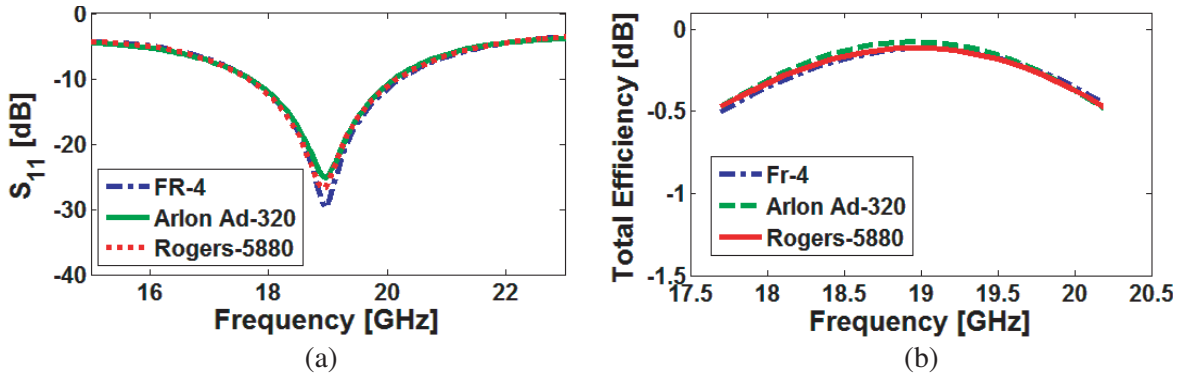


**Figure 5.** (a) Reflection coefficient ($S_{11}$) and (b) total efficiency of the antenna for different types of dielectrics.

($\delta = 0.0038$ & $\varepsilon_r = 3.2$), and Rogers-5880 ($\delta = 0.0009$ & $\varepsilon_r = 2.2$) are studied. It is shown in Fig. 5(a) that unlike the conventional antennas, the proposed air-filled loop array exhibits similar results and its reflection coefficient does not change for different types of substrate dielectrics [38]. The total efficiencies of the antenna design for different types of dielectrics are illustrated in Fig. 5(b). It should be noted the studied dielectrics have different values of loss tangent $\delta$ which could affect the efficiency of an antenna [39, 40]. However, as plotted in Fig. 5(b), the antenna provides a similar behavior with high efficiencies for different types of dielectrics.

## 3. CHARACTERISTICS OF THE 5G SMARTPHONE PHASED ARRAY

As illustrated in Fig. 6(a), eight identical dielectric-insensitive antenna elements are arranged a linear array antenna. The designed linear array has a low profile with the dimension of $W_a \times L_a = 8.5 \times 43\,\text{mm}^2$. Fig. 6(b) illustrates and compares the gain characteristic of the antenna element and the array design over the operation band of 18–20 GHz. As can be observed the antenna element can provide $3 \sim 5$ dBi maximum gains while the linear antenna array exhibits high gain levels (more than 1 dBi), over the antenna operation band.

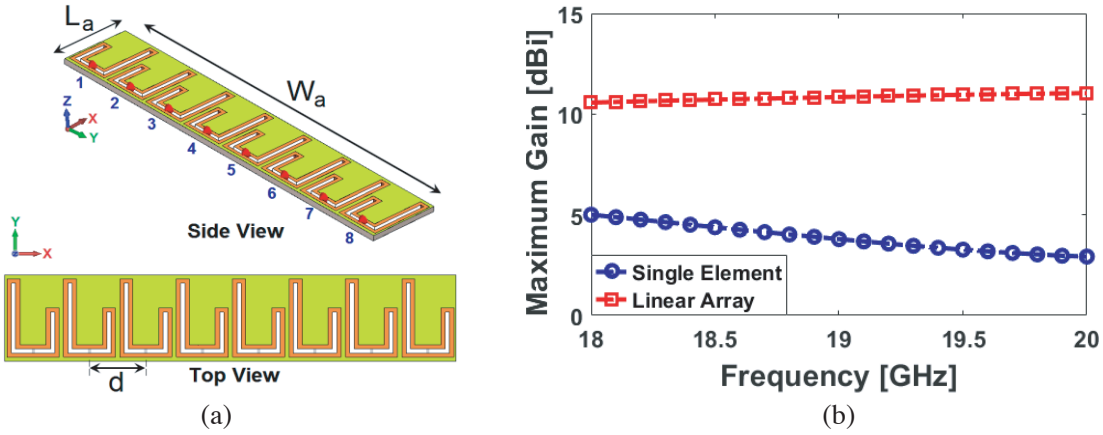


**Figure 6.** (a) Linear antenna array and (b) comparison of the gain levels for the single-element and the designed array.

The schematic of the proposed smartphone antenna array is represented in Fig. 7(a). It is seen that the designed linear array has been embedded at the top edge of the handset mainboard with an overall size of $W_{sub} \times L_{sub} = 55 \times 110\,\text{mm}^2$. Fig. 7(b) illustrates the $S$-parameters ($S_{11} \sim S_{81}$) of the phased array

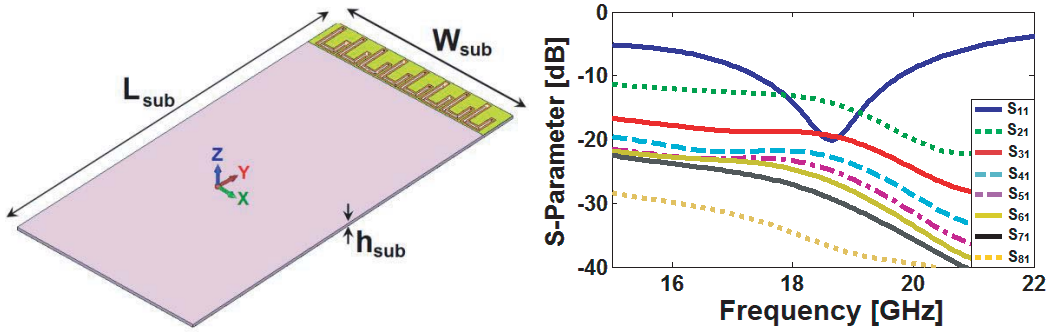


(a) (b)

**Figure 7.** (a) Configuration and (b) $S$-parameters of the antenna array.

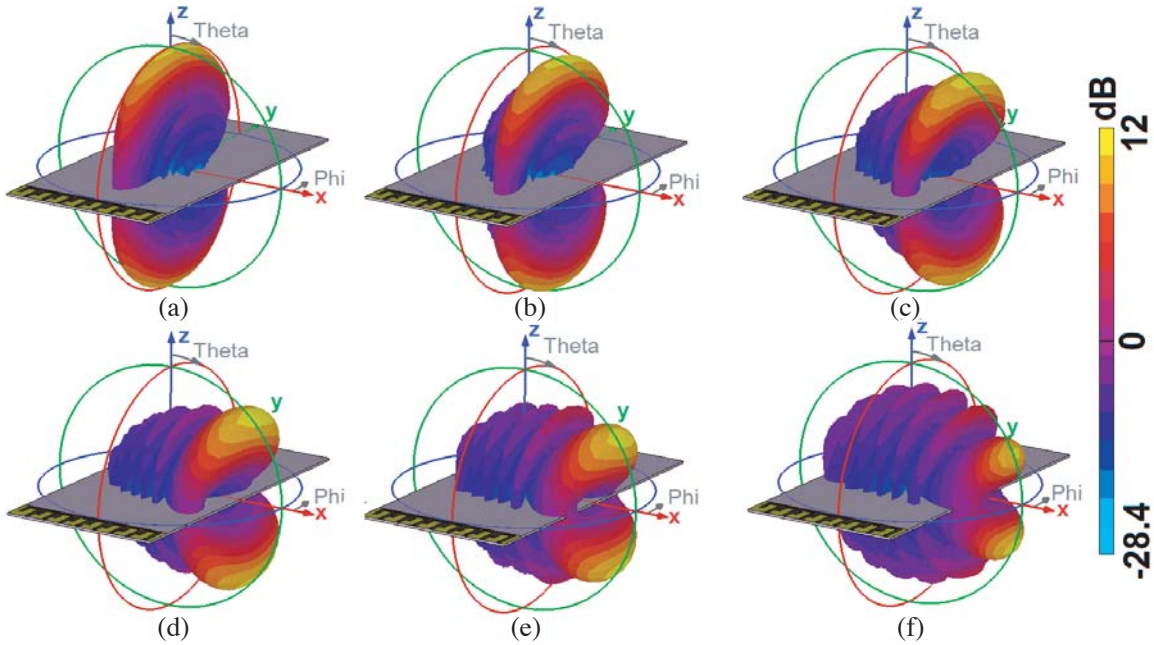


(a) (b) (c) (d) (e) (f)

**Figure 8.** Transparent radiation beams of the array at (a) 0°, (b) 15°, (c) 30°, (d) 45°, (e) 60°, and (f) 70°.

smartphone antenna. As illustrated, the antenna resonators of the smartphone antenna provide good $S_{nn}$ characteristics covering the frequency range of 18–20 GHz. Moreover, sufficient mutual coupling ($S_{mn} < -15$ dB) is observed among the antenna elements. Fig. 8 illustrates the 3D beam-steering of the array radiation at 19 GHz for wide scanning angles. As observed, the array exhibits quite good and well-defined beam steering over of 0–70 scanning angles. As shown, the design provides quasi end-fire and well-defined radiation beams at 0°, 15°, 3°, 45°, 60°, and 7° which could cover half-space of the radiation coverage for the smartphone mainboard [41–45].

Fundamental properties of the design including directivity, radiation, and total efficiencies for the steered beams of the mobile-phone array at 19 GHz design are presented in Fig. 9(a). Across the scanning range of 0° to 60°, the antenna radiation and total efficiencies are greater than 90% (−0.5 dB). Besides, for the scanning angle $\leq \pm 60$, the array directivity varies from 11 to 12 dB. Fig. 9(b) illustrates the realized gains of the proposed phased array antenna. As seen, the antenna has high gain levels at different angles. As shown, for the scanning range of 0 to 50 degrees, almost constant gains with values more than 10 dB are obtained [46–50].

The user-hand is a body-part that most frequently touches the handheld devices and usually has

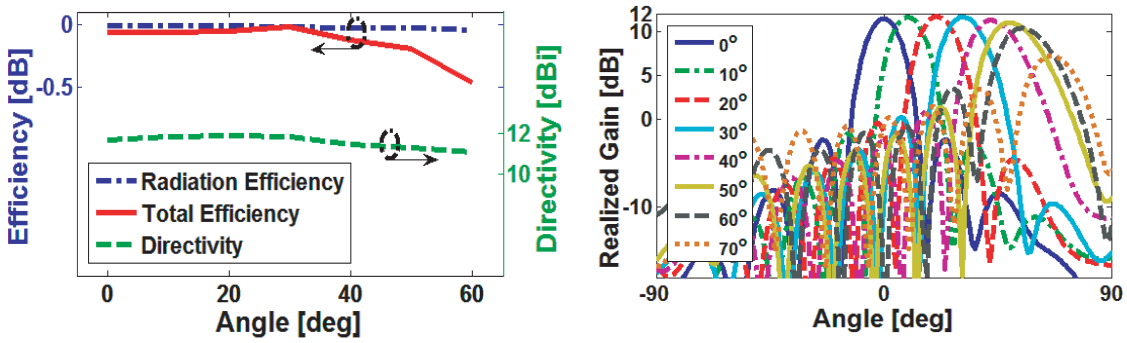


(a) (b)

**Figure 9.** (a) Fundamental radiation properties and (b) beam-steering function of the array at different scanning angles (0 to 60 degree).

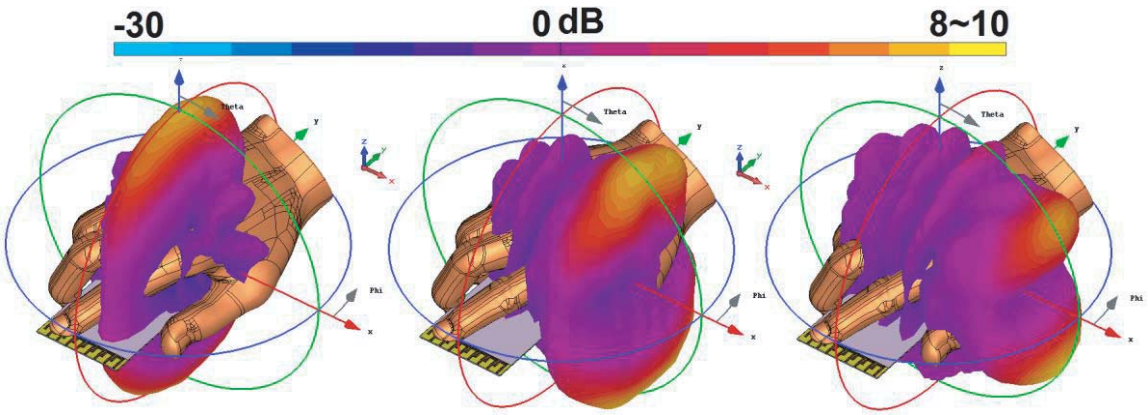


(a) (b) (c)

**Figure 10.** Simulated 3D radiation beams in Data-Mode at, (a) 0, (b) 30, and (c) 60 degrees.

negative impacts on antenna performance [51–53]. Fig. 10 plots the 3D patterns of the smartphone antenna radiation beams at 0°, 30°, and 60° angels. It is shown that the proposed dielectric-insensitive phased array offers good radiation behavior with sufficient gain levels and well-defined beam-steering characteristics. However, the gain levels of the proposed array are affected significantly owing to the

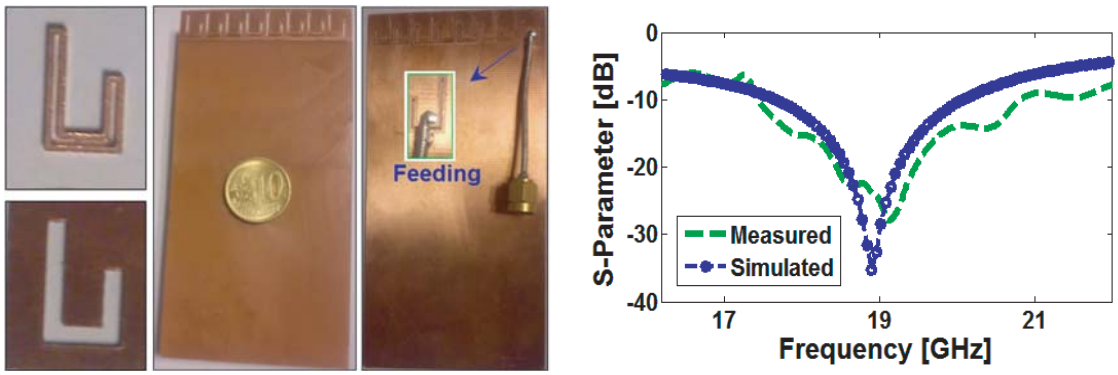


(a) (b)

**Figure 11.** (a) Single element, front/back views of the Fabricated prototype, (b) the reflection coefficient results.

absorption effect of the user's hand. This is because some EM energy has been absorbed by the hand.

Figure 11(a) shows the configuration of the fabricated antenna. During the fabrication, the L-shaped slots have been made in the dielectric and the L-ring metal loops are inserted into the slots. Due to similar performances of the radiation elements, the reflection coefficient ($S_{11}$) of the antenna element is measured for the proposed array and has been compared with the simulation in Fig. 11(b). As seen, the element exhibits sufficient measured/simulated $S_{11}$ with a good agreement. It can be seen the antenna has a good frequency response over the frequency range of 18 to 20 GHz. However, the fabricated antenna exhibits more than 2 GHz bandwidth. The measured and simulated antenna radiation patterns ($E$-plane and $H$-plane) for a single element of the smartphone antenna array have

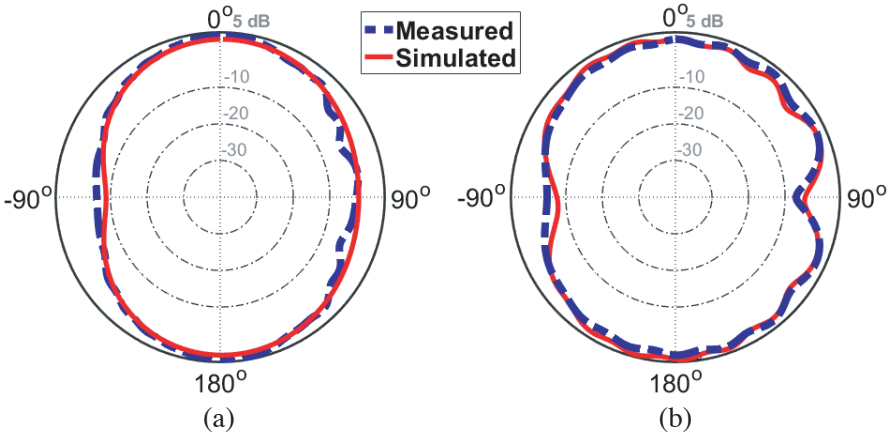


**Figure 12.** Measured and simulated radiation patterns of the antenna element at 19 GHz (resonance frequency), (a) $E$-plane and (b) $H$-plane.

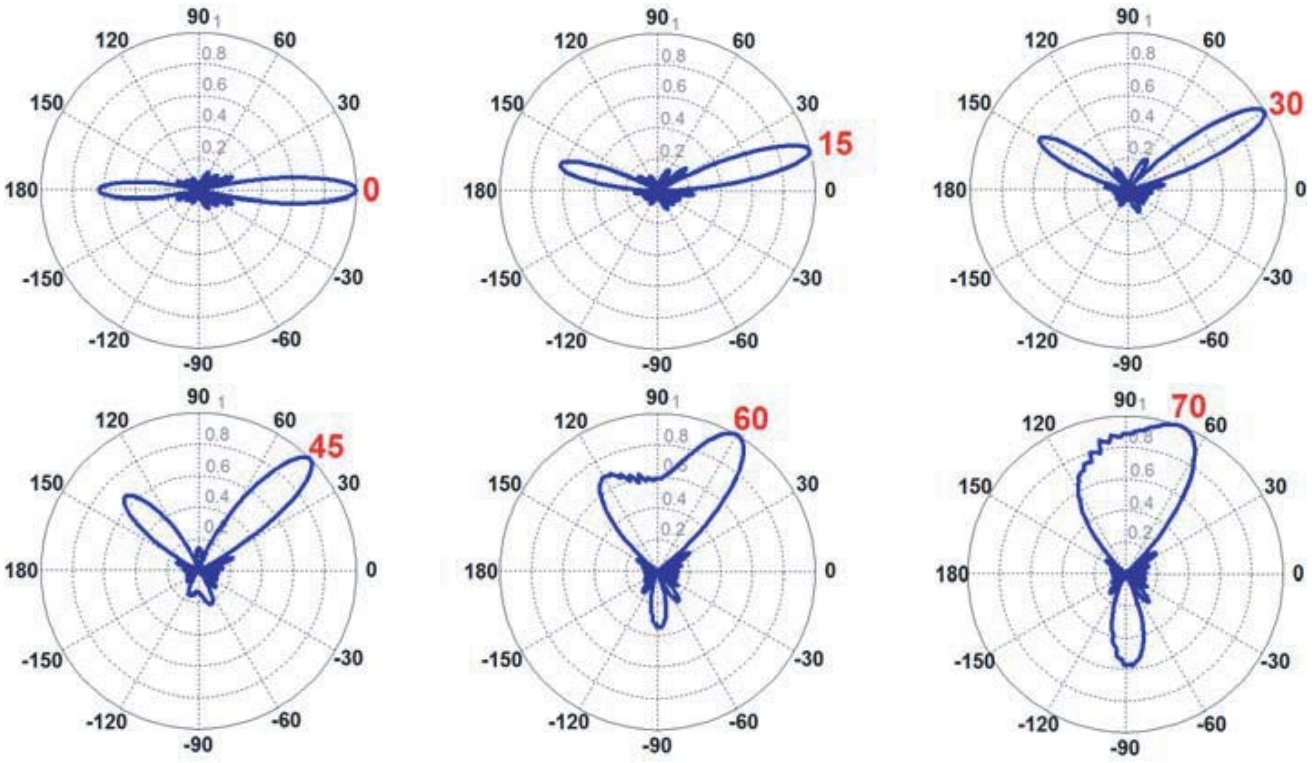


**Figure 13.** The synthesized beam patterns for different angles.

been illustrated in Fig. 12. The practical results show fair agreements with the simulated outcomes. As illustrated, the element provides a quasi-omnidirectional radiation pattern in $E$-plane [54–58]. The radiation's main direction ended in $H$-plane, as expected for quasi end-fire mode. In addition, as shown, the antenna is providing sufficient gain values at the centre frequency. Also, the normalized beam patterns of the linear array have been synthesized using the radiation pattern for the antenna element. The synthesized 2D-polar results are illustrated in Fig. 13 for a wide scanning range from 0° up to 70° [59, 60]. It is shown that good beam-steering characteristic is obtained.

## 4. CONCLUSION

In this manuscript, a new dielectric-insensitive antenna array is introduced for the upcoming 5G cellular communications. The proposed array is designed on the FR-4 dielectric and working in the frequency range of 18 to 20 GHz. Eight elements of metal-ring antenna elements were used in a linear array configuration on the top edge of the mobile phone PCB. The designed antenna array offers good features in terms of impedance bandwidth, efficiency, gain, and radiation beams.

## ACKNOWLEDGMENT

This work is supported by the European Union's Horizon 2020 research and innovation programme under grant agreement H2020-MSCA-ITN-2016 SECRET-722424.

## REFERENCES

1. Osseiran, et al., "Scenarios for 5G mobile and wireless communications: the vision of the METIS project," *IEEE Commun. Mag.*, Vol. 52, 26–35, 2014
2. Parchin, N. O., et al., *Microwave/RF Components for 5G Front-End Systems*, Avid Science, 2019.
3. Roh, W., et al., "Millimeter-wave beamforming as an enabling technology for 5G cellular communications: Theoretical feasibility and prototype results," *IEEE Commun. Mag.*, Vol. 52, 106–113, 2014.
4. Al-Yasir, Y. I. A., et al., "A new polarization-reconfigurable antenna for 5G applications," *Electronics*, Vol. 7, 1–9, 2018.
5. Parchin, N. O., et al., "UWB MM-wave antenna array with quasi omnidirectional beams for 5G handheld devices," *International Conference on Ubiquitous Wireless Broadband (ICUWB)*, Nanjing, China, 2016.
6. Ojaroudi Parchin, N., H. J. Basherlou, and R. A. Abd-Alhameed, "A design of crossed exponentially tapered slot antenna with multi-resonance function for 3G/4G/5G applications," *Progress In Electromagnetics Research Letters*, Vol. 92, 1–8, 2020.
7. Gupta, P., "Evolvement of mobile generations: 1G to 5G," *International Journal for Technological Research in Engineering*, Vol. 1, 152–157, 2013.
8. Ojaroudi Parchin, N., Y. I. A. Al-Yasir, H. J. Basherlou, and R. A. Abd-Alhameed, "A closely spaced dual-band MIMO patch antenna with reduced mutual coupling for 4G/5G applications," *Progress In Electromagnetics Research C*, Vol. 101, 71–80, 2020.
9. Parchin, N. O., et al., "Design of Vivaldi antenna array with end-fire beam steering function for 5G mobile terminals," *T*elecommunications Forum (TELFOR), 587–590, Belgrade, Serbia, Nov. 24–26, 2015.
10. Ojaroudiparchin, N., et al., "Low-cost planar mmWave phased array antenna for use in mobile satellite (MSAT) platforms," *Telecommunications Forum (TELFOR)*, 528–531, Serbia, 2015.
11. Chen, Q., Z. Gong, X. Yang, Z. Wang, and L. Zhang, "Design considerations for millimeter wave antennas within a chip package," *IEEE International Workshop on Anti-counterfeiting, Security, Identification*, 13–17, Xiamen, Fujian, Apr. 16–18, 2007.

12. Parchin, N. O., et al., "Frequency-switchable patch antenna with parasitic ring load for 5G mobile terminals," *IEEE International Symposium on Antennas and Propagation (ISAP)*, Xi'an, China, 2019.
13. Parchin, N. O., et al., "Frequency reconfigurable antenna array for MM wave 5G mobile handsets," *Broadband Communications, Networks, and Systems, BROADNETS*, Faro, Portugal, 2019.
14. NTT Docomo, "Docomo 5G White Paper," Jul. 2014 [Online], available: https://www.nttdocomo.co.jp/english/corporate/technology/whitepaper_5g/.
15. Parchin, N. O. and R. A. Abd-Alhameed, "A compact Vivaldi antenna array for 5G channel sounding applications," *EuCAP*, London, UK, 2018.
16. Parchin, N. O., et al., "MM-wave phased array quasi-yagi antenna for the upcoming 5G cellular communications," *Applied Sciences*, Vol. 9, 1–14, 2019.
17. Hong, W., K. Baek, Y. Lee, and Y. G. Kim, "Design and analysis of a low-profile 28 GHz beam steering antenna solution for future 5G cellular applications," *IEEE International Microwave Symposium*, Tampa Bay, Florida, Jun. 1–6, 2014.
18. Ojaroudiparchin, N., M. Shen, and G. F. Pedersen, "Multi-layer 5G mobile phone antenna for multi-user MIMO communications," *Telecommunications Forum (TELFOR 2015)*, Serbia, Nov. 2015.
19. Amitay, N., V. Galindo, and C. P. Wu, *Theory and Analysis of Phased Array Antennas*, Wiley-Interscience, New York, 1972.
20. Rajagopal, S., S. Abu-Surra, Z. Pi, and F. Khan, "Antenna array design for multi-gbps mmwave mobile broadband communication," *Proc. IEEE GLOBECOM'2011*, 1–6, Houston, Texas, USA, 2011.
21. Ojaroudiparchin, N., M. Shen, and G. F. Pedersen, "Beam-steerable microstrip-fed bow-tie antenna array for fifth generation cellular communications," *EuCAP 2016*, Switzerland, 2016.
22. Parchin, N. O., et al., "High-performance Yagi-Uda antenna array for 28 GHz mobile communications," *TELFOR 2019*, Belgrade, Serbia, Nov. 25–27, 2019.
23. Ullah, A., et al., "Coplanar waveguide antenna with defected ground structure for 5G millimeter wave communications," *IEEE MENACOMM'19*, Bahrain, 2019.
24. Ojaroudi Parchin, N., H. J. Basherlou, and R. A. Abd-Alhameed, "Dual circularly polarized crescent-shaped slot antenna for 5G front-end applications," *Progress In Electromagnetic Research Letters*, Vol. 91, 41–48, 2020.
25. Parchin, N. O., et al., "Reconfigurable phased array 5G smartphone antenna for cognitive cellular networks," *23th Telecommunications Forum, TELFOR 2019*, Belgrade, Serbia, Nov. 25–27, 2019.
26. Ojaroudiparchin, N., et al., "Wide-scan phased array antenna fed by coax-to-microstriplines for 5G cell phones," *MIKON Conference*, Rakow, Poland, May 2016.
27. Hong, W., et al., "mmWave phased-array with hemispheric coverage for 5th generation cellular handsets," *EuCAP*, 714–716, 2014.
28. Parchin, N. O., et al., "A beam-steerable antenna array with radiation beam reconfigurability for 5G smartphones," *EuCAP 2020*, Copenhagen, Denmark, 2020.
29. Ojaroudiparchin, N., M. Shen, and G. F. Pedersen, "A compact design of planar array antenna with fractal elements for future generation applications," *Applied Computational Electromagnetics Society (ACES) Journal*, 789–796, 2016.
30. CST Microwave Studio, ver. 2014, CST, Framingham, MA, USA, 2014.
31. Ojaroudi Parchin, N., R. A. Abd-Alhameed, and M. Shen, "Gain improvement of a UWB antenna using a single-layer FSS," *2019 Photonics & Electromagnetics Research Symposium — Fall (PIERS — Fall)*, Xiamen, China, Dec. 17–20, 2019.
32. Valizade, A., et al., "Band-notch slot antenna with enhanced bandwidth by using Ω-shaped strips protruded inside rectangular slots for UWB applications," *Appl. Comput. Electromagn. Soc. (ACES) J.*, Vol. 27, No. 10, 816–822, 2012.
33. Ojaroudi, N. and N. Ghadimi, "Design of CPW-fed slot antenna for MIMO system applications," *Microw. Opt. Technol. Lett.*, Vol. 56, 1278–1281, 2014.

34. Basherlou, H. J., et al., "MIMO monopole antenna design with improved isolation for 5G WiFi applications," *International Journal of Electrical and Electronic Science*, Vol. 7, 1–5, 2019.
35. Ojaroudi Parchin, N., H. J. Basherlou, and R. A. Abd-Alhameed, "UWB microstrip-fed slot antenna with improved bandwidth and dual notched bands using protruded parasitic strips," *Progress In Electromagnetic Research C*, Vol. 101, 261–273, 2020.
36. Yngvesson, K. S., et al., "The tapered slot antenna-a new integrated element for millimeter-wave applications," *IEEE Trans. Microw. Theory Techn.*, Vol. 37, 365–374, 1989.
37. Parchin, N. O., et al., "Low-profile air-filled antenna for next generation wireless systems," *Wirel. Pers. Commun.*, Vol. 97, 3293–3300, 2017.
38. Salman, J. W., M. M. Ameen, and S. O. Hassan, "Effects of the loss tangent, dielectric substrate permittivity and thickness on the performance of circular microstrip antennas," *Journal of Engineering and Development*, Vol. 10, No. 1, 1–13, 2006.
39. Ojaroudi, N. and M. Ojaroudi, "Bandwidth enhancement of an ultra-wideband printed slot antenna with WLAN band-notched function," *Microw. Opt. Technol. Lett.*, Vol. 55, 1448–1451, 2013.
40. Ojaroudi, M. and N. Ojaroudi, "Ultra-wideband slot antenna with frequency band-stop operation," *Microw. Opt. Technol. Lett.*, Vol. 55, 2020–2023, 2013.
41. Ojaroudi, N., "Small microstrip-fed slot antenna with frequency band-stop function," *21st Telecommunications Forum, TELFOR 2013*, Belgrade, Serbia, Nov. 27–28, 2013.
42. Ojaroudi, N., "Design of ultra-wideband monopole antenna with enhanced bandwidth," *21st Telecommunications Forum, TELFOR 2013*, Belgrade, Serbia, Nov. 27–28, 2013.
43. Ojaroudi, Y., et al., "Circularly polarized microstrip slot antenna with a pair of spur-shaped slits for WLAN applications," *Microw. Opt. Technol. Lett.*, Vol. 57, 756–759, 2015.
44. Ojaroudi, N., H. Ojaroudi, and N. Ghadimi, "Quadband Planar Inverted-F Antenna (PIFA) for wireless communication systems," *Progress In Electromagnetics Research Letters*, Vol. 45, 51–56, 2014.
45. Ojaroudiparchin, N., M. Shen, and G. F. Pedersen, "$8 \times 8$ planar phased array antenna with high efficiency and insensitivity properties for 5G mobile base stations," *Proc. 10th Eur. Conf. Antennas Propag. (EuCAP)*, 1–5, Davos, Switzerland, Apr. 2016.
46. Parchin, N. O., et al., "$8 \times 8$ MIMO antenna system with coupled-fed elements for 5G handsets," *IET Conference on Antennas and Propagation*, Birmingham, UK, Nov. 2019.
47. Parchin, N. O., R. A. Abd-Alhameed, and M. Shen, "A radiation-beam switchable antenna array for 5G smartphones," *2019 Photonics & Electromagnetics Research Symposium — Fall (PIERS — Fall)*, 1769–1774, Xiamen, China, Dec. 17–20, 2019.
48. Ojaroudiparchin, N., M. Shen, and G. F. Pedersen, "Investigation on the performance of low-profile insensitive antenna with improved radiation characteristics for the future 5G applications," *Microw. Opt. Technol. Lett.*, Vol. 58, 2148–2158, 2016.
49. Hansen, R. C., Phased Array Antennas, John Wiley & Sons, Inc., New York, 2009.
50. Parchin, N. O., et al., "Smartphone antenna design covering $2G \sim 5G$ mobile terminals," *International Journal of Electrical and Electronic Science*, Vol. 7, 1–6, 2020.
51. Parchin, N. O., R. A. Abd-Alhameed, and M. Shen, "Design of low cost FR4 wide-band antenna arrays for future 5G mobile communications," *International Symposium on Antennas and Propagation (ISAP)*, Xi'an, China, 2019.
52. Ilvonen, J., et al., "Mobile terminal antenna performance with the user's hand," *IEEE Antenna and Wireless Propagation Letters*, Vol. 10, 772–775, 2000.
53. Parchin, N. O., et al., "Multi-band MIMO antenna design with user-impact investigation for 4G and 5G mobile terminals," *Sensors*, Vol. 19, 456, 2019.
54. Ojaroudi, N., "Circular microstrip antenna with dual band-stop performance for ultra-wideband systems," *Microw. Opt. Technol. Lett.*, Vol. 56, 2095–2098, 2014.
55. Ojaroudi, M., et al., "Dual band-notch small square monopole antennawith enhanced bandwidth characteristics for UWB applications," *ACES J.*, Vol. 25, 420–426, 2012.

56. Siahkal-Mahalle, B. H., et al., "A new design of small square monopole antenna with enhanced bandwidth by using cross-shaped slot and conductor-backed plane," *Microw. Opt. Technol. Lett.*, Vol. 54, 2656–2659, 2012.
57. Ojaroudi, M., et al., "Ultra-wideband small square monopole antenna with dual band-notched function," *Microw. Opt. Technol. Lett.*, Vol. 54, 372–374, 2012.
58. Ojaroudi, N., et al., "Compact ultra-wideband monopole antenna with enhanced bandwidth and dual band-stop properties," *International Journal of RF and Microwave Computer-Aided Engineering*, Vol. 25, 346–357, 2015.
59. Parchin, N. O., et al., "Recent developments of reconfigurable antennas for current and future wireless communication systems," *Electronics*, Vol. 8, 128, 2019.
60. Ojaroudiparchin, N., et al., "A switchable 3-D-coverage-phased array antenna package for 5G mobile terminals," *IEEE Antennas Wireless Propag. Lett.*, Vol. 15, 1747–1750, 2016.